International Journal of Pharmaceutics 388 (2010) 213–222

Contents lists available at ScienceDirect

International Journal of Pharmaceutics

journal homepage: www.elsevier.com/locate/ijpharm

Pharmaceutical Nanotechnology

Analysis of phase diagram and microstructural transitions in an ethyl oleate/water/Tween 80/Span 20 microemulsion system using high-resolution ultrasonic spectroscopy

Sinead Hickey[a], Sue A. Hagan[b], Evgeny Kudryashov[a], Vitaly Buckin[a,*]

[a] School of Chemistry and Chemical Biology University College Dublin, Belfield, Dublin 4, Ireland
[b] Aphton Biopharma, Loughborough, London, UK

ARTICLE INFO

Article history:
Received 11 September 2009
Received in revised form
30 November 2009
Accepted 1 December 2009
Available online 16 December 2009

Keywords:
Microemulsion
Ultrasonic spectroscopy
HR-US
Particle size
Ultrasonic velocity
Ultrasonic attenuation
Phase diagram
Hydration

ABSTRACT

High-resolution ultrasonic spectroscopy was applied to analyse a pseudo-ternary phase diagram for a mixture consisting of water/ethyl oleate/Tween 80 and Span 20 at 25 °C. The measured changes in the ultrasonic velocity and attenuation with concentration of water in oil/surfactants mixtures showed several, well defined stages and transitions between them, which allowed construction of an 'ultrasonic' phase diagram. Quantitative analysis of the ultrasonic parameters enabled characterisation of various phases (microemulsion, liquid crystals and pseudo-bicontinuous) as well as evaluation of the state of the water and particle size in microemulsion phase.

1. Introduction

Microemulsions are homogenous, transparent, thermodynamically stable dispersions of water in oil or oil in water, stabilized by an interfacial film of surfactant, usually in combination with a co-surfactant (Warisnoicharoen et al., 2000). In contrast to the traditional emulsion they have a small droplet size (below 200 nm). Microemulsions have attracted considerable interest over past years as potential drug delivery systems due to their unique properties, such as stability, ease of preparation and their ability to form spontaneously (Lawrence and Rees, 2000; Gao et al., 1998; Patel et al., 2006; Narang et al., 2007).

Many techniques have been used in analysing microemulsions (Moulik and Paul, 1998). Light scattering is regularly employed (Aboofazeli and Lawrence, 1993; Aboofazeli et al., 2000; Hwang et al., 2004). Other scattering techniques such as X-ray diffraction and neutron scattering were successfully used in determining the phases and structural changes of the surfactant aggregates as well as detecting changes in the microstructure of microemulsions (Raman et al., 2003; Benjamins et al., 2005; Arleth and Pederson, 2001; Johannessen et al., 2004). Light and neutron scattering techniques generally require dilution of concentrated samples or complicated calculations in order to obtain reliable estimates of the particle sizes of the system. The dilution of a microemulsion containing a co-surfactant often leads to a change in either the microstructure of the system, or in extreme cases, the disappearance of the microemulsion droplets (Hou et al., 1988; Coupland and McClements, 2001). Microemulsions have also been characterised by measuring their electrical properties using conductivity or electroacoustic techniques (Jian et al., 2001; Dukhin et al., 2000); however, these last techniques are often limited to charged particles in a conducting medium.

Developing of microemulsion based formulations requires techniques that allow the user to analyse their microstructure and the conditions at which they are formed (including analysis of phase diagrams, particle size, and hydration effects, etc.). Ultrasonic spectroscopy has a considerable potential in this area as demonstrated previously (Lang et al., 1980; Ballaro et al., 1980; Mehta and Kawaljit, 1998; Wines et al., 1999; Letamendia et al., 2001). This technique employs an ultrasonic wave (MHz frequency acoustical waves), which probes the elastic rather than electric and magnetic characteristics of materials. As it transverses a sample, compressions and decompressions in the ultrasonic wave change

* Corresponding author. Tel.: +353 1 716 2371; fax: +353 1 716 1178.
E-mail address: vitaly.buckin@ucd.ie (V. Buckin).

0378-5173/$ – see front matter © 2009 Elsevier B.V. All rights reserved.
doi:10.1016/j.ijpharm.2009.12.003

the distance between molecules within the sample, which in turn respond by intermolecular repulsions and attractions. This ability of ultrasonic waves to probe intermolecular forces allows access to molecular levels of organisation. Measurements of scattering effects of ultrasonic waves allow particle size analysis.

The use of ultrasonic spectroscopy in microemulsion systems in the past has been limited by low resolution and requirements of large sample volumes. However, this was overcome with the introduction of high-resolution ultrasonic spectroscopy (HR-US) (Buckin and O'Driscoll, 2002; Buckin et al., 2003, 2002a,b; Kudryashov et al., 2000). A variety of pharmaceutical and biochemical structures have previously been successfully characterised using HR-US. These include monitoring of immunochemical reactions (Buckin and Kudryashov, 2002), gelatinisation of starch (Lehmann et al., 2004), crystallisation of proteins (Smyth et al., 2003) and the characterisation and determination of particle size of emulsions (Buckin et al., 2002a,b; Smyth et al., 2004) and other micelle systems (Buckin et al., 2002a,b; Kudryashov et al., 1998; Smyth et al., 1999).

Recently, we applied high-resolution ultrasonic spectroscopy for analysis of phase diagrams in microemulsion systems consisted of pharmaceutically acceptable ingredients such as water/isopropyl myristate/epikuron200/*n*-propanol (Hickey et al., 2006). Quantitative analysis of the ultrasonic parameters measured in the samples with different ratios of oil/surfactant at varied water content enabled characterisation of various phases: swollen micelles, microemulsion, coarse emulsion, liquid crystal and pseudo-bicontinuous phases as well as evaluation of the state of water in emulsion droplets and characterisation of the size of the droplets. It was found that the compressibility of water in microemulsion droplets (diameter 10 nm and larger) is close to the compressibility expected for the droplets containing bulk water.

This paper describes the application of HR-US for analysis of the phase transitions and phase diagram of a different system consisting of an oil (ethyl oleate), surfactants (sorbitan mono-laurate (Span 20) and poly(oxyethylene 20) sorbitan mono-oleate (Tween 80)), and water. This system does not contain co-surfactant, but includes two different surfactants, Span 20 and Tween 80. We measured the changes in the ultrasonic velocity and in the ultrasonic attenuation when the oil and surfactants were titrated with water. These changes showed several well defined patterns (stages), which were related to the microstructural state of the samples. An 'ultrasonic' phase diagram was constructed from the ultrasonic titration profiles and compared with one obtained by Alany et al. (2001) using viscosity, conductivity, freeze-fracture transmission electron microscopy, phase-contrast and polarizing light microscopy. The particle size in the microemulsion region was estimated using the thermo-physical properties of the dispersed water phase and continuous oil and surfactants phase.

2. Experimental

2.1. Materials

Ethyl oleate (Cat. no. 27,074-1), sorbitan mono-laurate (Span 20, Cat. no. 1338-39-2) and polyoxyethylene 20 sorbitan mono-oleate (Tween 80, Cat. no. 9005-65-6) were purchased from Sigma Aldrich Ireland Ltd. (Dublin, Ireland). All reagents were of the highest purity available and were used as received. The ultrapure water (Millipore Super-Q-System) with the conductivity of 18.2 M cm^{-1} was used in sample preparation. All samples were prepared by weight. The temperature was kept constant at 25 °C using a Haake F8 waterbath with a stability of ±0.01 °C.

2.2. Ultrasonic measurements

Ultrasonic velocity (u) and ultrasonic attenuation (α) measurements were performed within 2 to 12 MHz frequency range using a HR-US 102 instrument (Ultrasonic Scientific Ltd.). This device is equipped with two cells enabling measurements to be performed in a single cell or differentially using two cells. The differential regime allows a resolution of 0.2 mm/s for the ultrasonic velocity and 0.2% for ultrasonic attenuation. Single cell measurements were performed in this work as the top resolution was not required. This gave a reproducibility of 1 cm/s for ultrasonic velocity and 0.4% for ultrasonic attenuation. The appropriate amounts of sorbitan mono-laurate and polyoxyethylene 20 sorbitan mono-oleate (2:3 ratio) and ethyl oleate were weighed into screw-capped vials. The samples were stirred until a clear solution was obtained. They were then placed into a syringe along with a magnetic stirrer and degassed by placing under vacuum over a stirring plate. 1.3 mL of each sample was placed in the HR-US 102 cell using a calibrated Hamilton syringe. An automated Hamilton dispenser (series 500) and 100 μL Hamilton syringe were used for the titrations. Measurements of the ultrasonic velocity and attenuation were executed while the sample was titrated with aliquots of degassed water through a septum in the lid of the cell. The samples were stirred at the bottom of the cell using the built-in HR-US digital stirring system and at the top of the cell using a mechanical mini stirrer. This provided fast, effective and homogeneous stirring. The stirring was continued after each addition of water until no further change in the ultrasonic velocity and attenuation occurred, indicating equilibrium had been reached. In addition, ultrasonic titration profiles were verified by the measurement of ultrasonic parameters in samples that were individually prepared and equilibrated over several hours before being placed in the HR-US cell. Because of the high viscosity of the samples in the range of concentrations of water corresponding to the stage III on the phase diagram, which prevented effective stirring at room temperature the samples were heated to 45 °C to enable the homogenous mixing of added water and cooled down to 25 °C before measurements. The ultrasonic velocity and attenuation profiles are shown in Figs. 1–3.

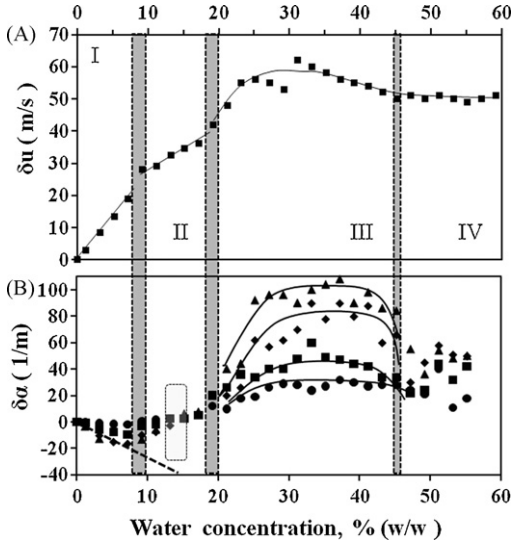

Fig. 1. Ultrasonic titration profiles for 25 wt% ethyl oleate and 75 wt% Tween 80:Span 20 (3:2) mixture at 25 °C. (A) Ultrasonic velocity profile at 5.2 MHz. (B) Ultrasonic attenuation profiles at four frequencies: (●) 2.7 MHz, (■) 5.2 MHz, (♦) 8.5 MHz and (▲) 11.7 MHz. Solid lines at the stage III are used as guidelines only. Dotted line represents the change in ultrasonic attenuation in sample at 11.7 MHz calculated using additive scheme according to Eq. (1) with $\alpha_S = 0$. The data within selected oval region were used in the estimation of particle size.

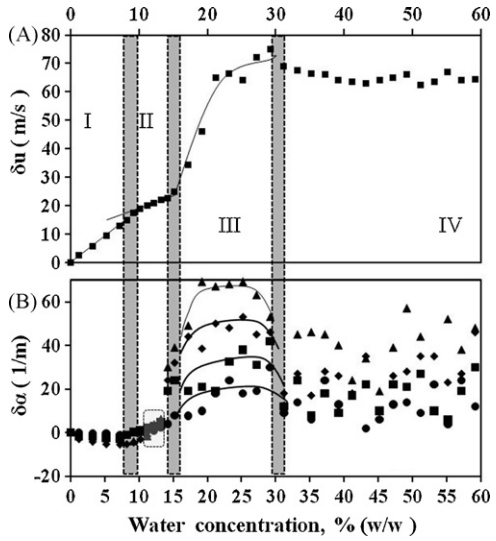

Fig. 2. Ultrasonic titration profiles for 50 wt% ethyl oleate and 50 wt% Tween 80:Span 20 (3:2) mixture at 25 °C. (A) Ultrasonic velocity profile at 5.2 MHz. (B) Ultrasonic attenuation profiles at four frequencies: (●) 2.7 MHz, (■) 5.2 MHz, (♦) 8.5 MHz and (▲) 11.7 MHz. The data within oval region were used in the estimation of particle size using PSize software module. Solid lines at the stage III are used as guidelines only.

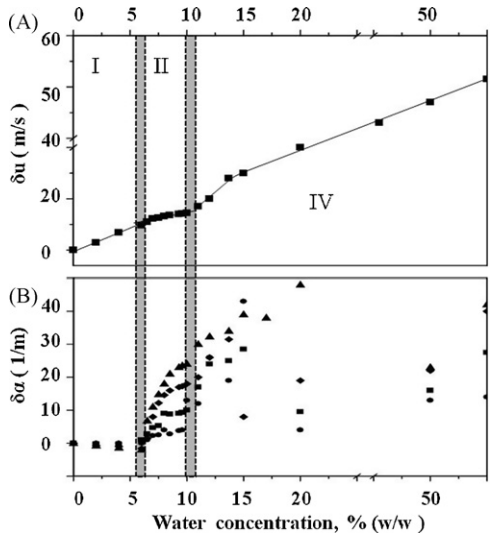

Fig. 3. Ultrasonic titration profiles for 75 wt% ethyl oleate and 25 wt% Tween 80:Span 20 (3:2) mixture at 25 °C. (A) and (B) Ultrasonic velocity profile at 5.2 MHz. (B) Ultrasonic attenuation profiles at four frequencies: (●) 2.7 MHz, (■) 5.2 MHz, (♦) 8.5 MHz and (▲) 11.7 MHz.

2.3. Density

The densities of the various ethyl oleate/Tween 80/Span 20 solutions were measured using a vibrating tube densimeter (DMA-602, Anton Paar, Austria) with a resolution of $\pm 1.5 \times 10^{-6}$ g cm^{-3}. 1 mL of each solution was degassed and placed in the densimeter. The temperature was controlled using a Haake F8 waterbath which provided control within of ±0.01 °C. Measurements were made at 15, 25 and 35 °C and the density and thermal expansion coefficients were calculated.

2.4. Differential scanning calorimetry

The specific heat capacities of the various ethyl oleate/Tween 80/Span 20 solutions were measured using a DSC 2010 Differential Scanning Calorimeter (TA Instruments). 10.5 mg of degassed sample was weighed into an aluminium crucible and placed in the sample holder. Measurements of specific heat capacity were carried out for each ratio of ethyl oleate/Tween 80/Span 20 using water as a reference from 0 to 40 °C at a ramp rate of 1 °C/min.

2.5. Thermal conductivity

Thermal conductivity measurements were carried out using a thermal conductivity probe constructed by Dr James Lyng of the Department of Food Science, UCD (Lyng et al., 2002). The probe was placed into a plastic cup containing approximately 50 mL of sample. The ratio of heat flux density to temperature gradient (over a 10 °C temperature range) was measured.

2.6. Dynamic light scattering (DLS)

DLS experiments were carried out with Zetasizer 3000 HSA (Malvern Instruments, UK). The system included an optical unit with a 10 W max output He–Ne laser with wavelength of the laser beam of 633 nm, and a Malvern K7132 correlator used in serial configuration. The quartz cell (12 mm) containing 2 mL sample was thermostated by build in Joule-Peltier thermostat at 25 °C. Microemulsion samples were prepared by adding of water droplet to 50:50 (w/w) of ethyl oleate and surfactants mixtures of Tween 80:Span 20 (3:2) and then dispersing it by gentle stirring, in order to get the final composition. Before measurement, the samples were filtrated through 0.02-μm membrane filters (Anotop 10, Whatman).

The mean (*Z* average) diameter of nanoparticles was measured at an angle detection of 90° using viscosity of the continuous medium of 62 mPa s (Table 1) and refractive indexes of 1.33 and 1.46 for the dispersant and dispersed phase, respectively. Each value was the mean of 3 measurements of 5000 s each, divided into 10 sub-runs. The particle diameter was determined from the autocorrelation function of the intensity of light scattered from the particles

Table 1
Thermo-physical properties of the dispersed water, and continuous phase, ethyl oleate:Tween 80 and Span 20 (3:2) at 25 °C used for particle size calculations.

Physical property	Water[a]	75:25 ethyl oleate:Span 20/Tween 80	50:50 ethyl oleate:Span 20/Tween 80	25:75 ethyl oleate:Span 20/Tween 80
Density, ρ (kg m^{-3})	997	908.1 ± 0.1	955.3 ± 0.1	1007.0 ± 0.1
Ultrasonic velocity, u (m s^{-1})	1497	1393.4 ± 0.5	1417.5 ± 0.5	1452.4 ± 0.5
Ultrasonic attenuation coefficient, α/f^2 ($\times 10^{-13}$ m^{-1}s^2)	0.225	6.2 ± 0.2	8.7 ± 0.5	17 ± 1
Viscosity (Pa s)	0.000895	0.021 ± 0.001	0.062 ± 0.002	0.173 ± 0.009
Thermal conductivity, γ (J(m s K)$^{-1}$)	0.5952	0.12 ± 0.02	0.12 ± 0.02	0.12 ± 0.02
Thermal expansion coefficient, e/ν ($\times 10^{-4}$ K^{-1})	2.57	7.54 ± 0.08	7.87 ± 0.08	7.86 ± 0.08
Specific heat, c_P (J kg^{-1} K^{-1})	4180	1784 ± 50	2161 ± 50	2349 ± 50

[a] Reference: Herrmann and Mc Clements (1999). The thermal properties of the oil/surfactants were measured in our laboratory using the techniques described in the text.

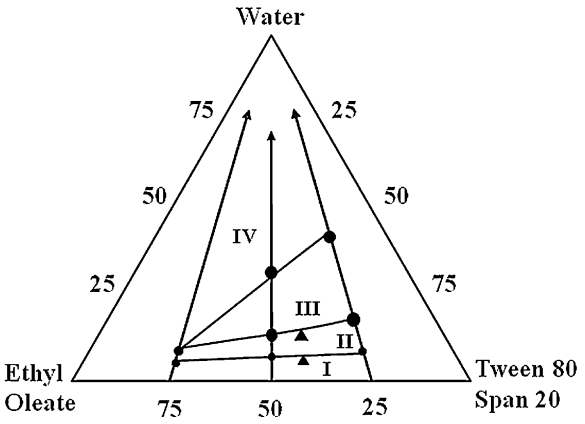

Fig. 4. Pseudo-ternary phase diagram of water/ethyl oleate/Tween 80 and Span 20 (3:2) at 25 °C. The arrows represent the ultrasonic titration path. The points connected by the line represent phase changes observed in the ultrasonic titration profiles. The filled triangles represent the transitions observed by Alany et al. (2001) using viscosity and conductivity measurements.

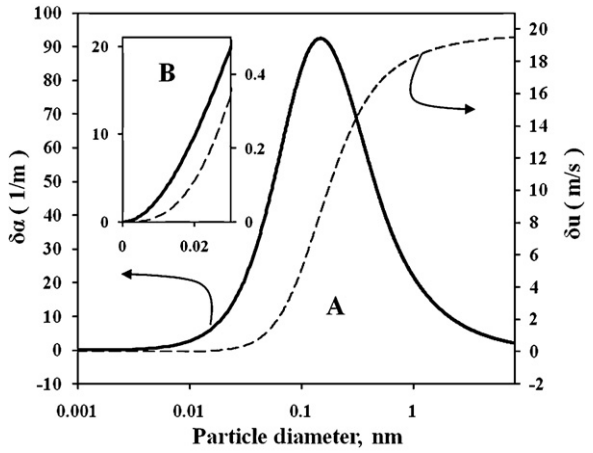

Fig. 5. (A) The predicted change in ultrasonic parameters with particle size for the mixture of 25:75 ethyl oleate:Tween 80 and Span 20 (3:2) and water content of 14 wt%, at 5.2 MHz and 25 °C calculated with the HR-US PSize software using the physical properties for the continuous and dispersed phases given in Table 1. (B) Zoom to the initial part of the ultrasonic curves.

using build in software provided with Zetasizer. The correction of determined particle size for hydrodynamic interactions between particles in microemulsion has been made using the procedure applied previously (Aboofazeli et al., 2000; Cheung et al., 1987). Our results showed that particle size measured in microemulsion at water fraction of 10 wt% is underestimated by 15% approximately.

2.7. Construction of pseudo-ternary phase diagrams

A phase diagram was constructed (Fig. 4) indicating phase transition points for various water/oil/surfactant concentrations. In order to show variation of composition of ethyl oleate/Tween 80/Span 20/water mixture on the phase diagram, the top apex of the triangle represents the water, while the other apices represent oil and surfactants concentrations.

2.8. Titration profile for ultrasonic attenuation. Particle sizing

The attenuation in emulsions, α, is represented by contributions of two terms: intrinsic absorption, α_I, and 'scattering' losses, α_S ($\alpha = \alpha_I + \alpha_S$; see for example Povey, 1997). For ideal dispersion the intrinsic absorption is a sum of attenuations in the continuous phase α_{I_0} and the dispersed phase (solute), $\alpha_{I_{solutes}}$, weighted according to their volume fractions and therefore:

$$\alpha = \alpha_{I_0}(1-x) + \alpha_{I_{solute}}x + \alpha_S \quad (1)$$

where x is the volume fraction of the dispersed phase, which is related to the mass fraction of the dispersed phase, w, according to:

$$x = w\frac{\nu_{solute}}{\nu_0}\frac{1}{1+w((\nu_{solute}/\nu_0)-1)} \quad (2)$$

where solute $\nu_{solute}(\equiv 1/\rho_{solute}$, ρ_{solute} is the density of the dispersed phase) and $\nu_0(\equiv 1/\rho_0$, ρ_0 is the density of the continuous phase).

The 'scattering' contribution to ultrasonic attenuation, α_S, is a function frequency, particle size and concentration and can be determined from ultrasonic scattering theories. In the long wavelength limit, i.e. when the wavelength of ultrasound (λ) is much longer than the particle radius (r), explicit expressions for the ultrasonic scattering in dispersions of spherical particles have been derived (Epstein and Carhart, 1953; Waterman and Truell, 1961; Allegra and Hawley, 1972; Povey, 1997). The basic mechanism of interaction of the ultrasonic wave with particles in dispersions in this regime contains two major contributors, thermoelastic and viscoinertial 'scattering'. These contributions result from the 'scattering' of the incident ultrasonic waves into the thermal and the viscous waves on the border between the particle and the continuous medium. In emulsions the thermoelastic mechanism dominates as the difference in density of the continuous and dispersed phases are not significant (Povey, 1997). This was confirmed by our estimations made with the PSize software module and physical parameters of our systems. The PSize software module (v. 2.28.01) provided with HR-US 102 spectrometer (Ultrasonic Scientific Ltd.) utilises widely accepted scattering theoretical approaches developed over the last forty years (see for example Epstein and Carhart, 1953; Waterman and Truell, 1961; Allegra and Hawley, 1972; Povey, 1997; Austin et al., 1996). This allows calculation of particle sizes in emulsions and suspensions and other colloidal systems based on the measured attenuation values and the thermophysical parameters of the continuous medium and the particles. In addition, it allows calculations of the changes in ultrasonic velocity and attenuation caused by the scattering effects for particles of a given size.

The required thermal parameters for the dispersed and continuous phase at 25 °C obtained as described above are shown in Table 1. These parameters were used in the estimation of the particle size (diameter) in the microemulsion from the measured slope of concentration dependence of attenuation, and also for the simulation of the dependence of attenuation and velocity on the particle size. An example of the simulated profile for ultrasonic parameters is given in Fig. 5. As can be seen from the figure the 'scattering' contribution to both parameters becomes to be negligibly small (compared with the effects observed) at sizes smaller than 4 nm approximately. This conclusion does not depend on the exact values physical properties of the continuous and the dispersed phases.

2.9. Titration profile for ultrasonic velocity. Partial concentration increment of the ultrasonic velocity

The state of water in microemulsion can be assessed through comparison of the measured slope of ultrasonic velocity (u) vs. concentration with the slope expected for an 'ideal' mixture where water in dispersed particles has the same physical properties as pure bulk water. In liquids with low ultrasonic attenuation (attenuation, α, per wavelength, λ, is significantly smaller than 1, $\alpha\lambda \ll 1$) the ultrasonic velocity is determined by their density, ρ,

and adiabatic compressibility (Urick, 1947):

$$u = \frac{1}{\sqrt{\beta_S \rho}} \tag{3}$$

where $\beta_S (\equiv -1/V(\partial V/\partial P)_S)$ is the coefficient of adiabatic compressibility, which determines the relative change of the volume, $(-\partial V/V)$ with applied excess pressure (∂P) in adiabatic compression in ultrasonic wave. In dispersions of small particles with the size much smaller than the wavelength of the ultrasonic wave (0.1–0.7 mm for our frequency range), the thermoelastic scattering affects the adiabatic compressibility and the viscoelastic scattering affects the density ('inertial' density) (Povey, 1997). However because the viscoelastic scattering in our systems is small and can be neglected, the 'inertial' density in Eq. (3) is the same as the 'gravitational' density and it can be calculated as an additive sum of contributions of continuous medium and the dispersed phase (solute): $\rho = \rho_o(1-\chi) + \rho_{solute}\chi$.

When analysing the concentration dependence of ultrasonic velocity, it is useful to express the values of β_S and ρ in Eq. (3) through the parameters, which have an additive thermodynamic sense, specific volume ν $(\equiv 1/\rho$, volume of unit of mass) and specific adiabatic compressibility, k_S $(\equiv \nu\beta_s$, compressibility of a unit of mass). This provides the following relationship for ultrasonic velocity:

$$u = \frac{\nu}{\sqrt{k_S}} \tag{4}$$

For a liquid mixture consisting of a solute (particle in our case) and a solvent (continuous medium), the specific volume and compressibility can be expressed in terms of apparent specific volume of the solute, φV, and apparent specific adiabatic compressibility of the solute, φK_s, defined as:

$$\varphi V = \frac{V - V_0}{m} \tag{5a}$$

$$\varphi K_S = \frac{K_S - K_{S_0}}{m} \tag{5b}$$

where V is the volume of the mixture, V_0 is the volume of pure solvent before mixing, K_S $(\equiv -(\partial V/\partial P)_S)$ is the adiabatic compressibility of the mixture, K_{S_0} $(\equiv -(\partial V_0/\partial P)_S)$ is the adiabatic compressibility of a pure solvent, m is the mass of the solute in the mixture. Following the above definitions of φV and φK_s, the specific volume and adiabatic compressibility of a mixture can be expressed as a sum:

$$\nu = \nu_0(1-w) + w\varphi V \tag{6a}$$

$$k_S = k_{S_0}(1-w) + w\varphi K_S \tag{6b}$$

where w is the mass fraction of the solute in the mixture. Combination of Eqs. (4)–(6) provides the following relationship for concentration (w) dependence of ultrasonic velocity in a mixture:

$$u = \frac{\nu_0 + w(\varphi V - \nu_0)}{\sqrt{k_{S_0} + w(\varphi K_S - k_{S_0})}} = u_0 \left(1 + w\frac{(\varphi V/\nu_0 - 1)}{\sqrt{1 + w(\varphi K_S/k_{S_0} - 1)}}\right) \tag{7}$$

where u_0 is the ultrasonic velocity in the continuous media. In ideal mixtures φV is the specific volume of the solute, ν_{solute}, which does not depend on concentration, w.

Scattering effect on compressibility (thermoelastic scattering) is originated by the difference in the amplitude of the temperature oscillation in the dispersed particle and the continuous medium in a course of adiabatic compressions in ultrasonic wave. The heat exchange between the particle and the continuous medium, caused by the temperature gradient at their border, affects the 'macroscopic' (within the length scale of ultrasonic wavelength) adiabatic compressibility of the mixture. Therefore the value of φK_S is a function of ratio of the size of particles and the wavelength of the heat wave, as this ratio determines the extent of the heat exchange between the particle/interface layer and its environment. Two limited cases can be distinguished. The first is the thermal low frequency limit corresponding to the size of the droplets much less than the wavelength of the heat wave generated on the surface of the droplets. At this limit the compressions in ultrasonic wave are so slow that the complete thermal equilibration occurs between the particle and its environment. The second is the thermal high-frequency limit, which is realised when the size of the droplets is much larger than the wavelength of the heat wave. At this limit the compressions in ultrasonic wave are too fast for a heat exchange between the particles and the continuous medium and adiabatic conditions are preserved for both the dispersed and the continuous medium.

The concentration dependence of φK_s at the low thermal frequency limit can be expressed in thermodynamic terms and is given by the following equation (Hickey et al., 2006):

$$\varphi K_S^0 = \varphi K_T - \frac{e_0^2 T}{c_{P_0}} \times \left[\frac{2\rho_0(\varphi E/e_0 - \varphi C_p/c_{p_0}) + w[\varphi C_p/c_{p_0} - 2\varphi E/e_0 + (\varphi E/e0)^2]}{1 - w + w\varphi C_p/c_{p_0}}\right] \tag{8}$$

where φK_T $(K_T \equiv -(\partial V/\partial P)_T)$ is the apparent specific isothermal compressibility, φE $(E \equiv (\partial V/\partial T)_P)$ is the apparent specific heat expansion and φC_p is the apparent specific heat capacity of the solute, T is the temperature (in K), e_0 is the specific heat expansion (change of specific volume per 1 K) of the continuous phase and c_{p_0} is the specific heat capacity of the continuous phase. The values of φK_T, φE and φC_p are defined as per Eq. (5) where K (or V) shall be substituted by an appropriate thermodynamic characteristic. Eq. (8) is a consequence of Eq. (5), the definitions of the apparent isothermal compressibility, apparent heat expansion and apparent heat capacity and the basic relationship between the adiabatic and isothermal compressibility:

$$\beta_s = \beta_T - \frac{e^2 T}{c_p} \tag{9}$$

where e, c_p and ρ are the specific heat expansion, the specific heat capacity at a constant pressure and the density of material, respectively. In the case of ideal mixtures the specific apparent values φK_T, φE and φC_p represent corresponding specific isothermal compressibility, specific heat expansion and specific heat capacity of pure solute (water in our case):

$$\varphi K_T = k_{T_{solute}}; \quad \varphi E = e_{solute}; \quad \varphi C_p = c_{P_{solute}} \tag{10}$$

At high thermal frequency limit the apparent adiabatic compressibility of the solute in ideal mixture, φK_s^∞ is given by $\varphi K_s^\infty = k_{S\,solute}$.

Eqs. (6)–(10) allow calculations of ultrasonic velocity in ideal mixtures for the thermal low frequency limit. The range of the sizes of water droplets corresponding to the thermal high and low frequency limits can be estimated from the wavelength of the heat wave, generated on the surface of the particles, λ_T:

$$\lambda_T = 2\sqrt{\frac{\pi\gamma}{f\rho c_p}} \tag{11}$$

where γ is the thermal conductivity of the medium and f is the frequency. For our system the wavelength was in the range from 50 to 100 nm. Therefore, microemulsions with a particle size of the order of 10 nm or less correspond to the thermal low frequency limit of ultrasonic velocity and emulsion droplets above 1 μm corresponds

Table 2
The partial concentration increment of ultrasonic velocity, a', in ethyl oleate:Tween 80 and Span 20:water microemulsion at various ratios of oil/surfactant at 25 °C.

Phase	75:25 oil:surf	50:50 oil:surf	25:75 oil:surf
I	0.09 ± 0.01	0.13 ± 0.02	0.16 ± 0.02
Low frequency limit[a]	−0.08	−0.04	−0.04
II	0.06 ± 0.02	0.08 ± 0.02	0.09 ± 0.02
Low frequency limit[a]	−0.06	−0.02	−0.02

[a] Partial concentration increment of the ultrasonic velocity of (bulk) water droplets calculated using Eqs. (7) and (8) and concentration of water corresponding to the middle of the appropriate stage.

to the thermal high-frequency limit. More accurately transitions between the thermal low and high-frequency limit cases can be described by the scattering theories. Fig. 5 represents the calculated dependence of ultrasonic velocity on the size of water droplets at constant volume fraction. These calculations qualitatively confirm the above conclusions.

For quantitative analysis of the state of added water the partial specific concentration increment of the ultrasonic velocity, a', at various water concentrations in the system (Table 2) was calculated using the following equation:

$$a' = \frac{\delta u}{u \delta w} \tag{12}$$

where $\delta u/\delta w$ is the slope of ultrasonic velocity with concentration, w (weight fraction of water). The experimental values of a' were then compared with predicted values for the thermal low and high-frequency limits of the ideal mixture to evaluate the state of water in this system.

3. Results

The change in the ultrasonic velocity and attenuation due to the addition of water to various ratios of ethyl oleate:Tween 80/Span 20 (3:2), at 25 °C is shown in Figs. 1–3. The ultrasonic velocity (Figs. 1–3(A)) did not show a significant dependence on frequency within the resolution of measurement at stages I and II and therefore, for clarity, data for one frequency, 5.2 MHz, are shown. At high water content (>25 wt%) some frequency dependence of the ultrasonic velocity has been detected, which will be subject of further studies. The ultrasonic attenuation does show a frequency dependence over whole concentration range of water, therefore a number of different frequencies between 2 and 12 MHz are plotted (Figs. 1–3(B)).

Several stages of microstructural rearrangement (I–IV) can be resolved from the concentration profiles of ultrasonic velocity and attenuation in Figs. 1–3. The transitions between stages are clearly indicated by break points in ultrasonic velocity profiles, where the slope of the velocity demonstrates an abrupt change as well as by sharp changes in attenuation profiles. Each stage shows similar features in profiles the ultrasonic curves at all three ratios of oil/surfactant.

3.1. 25:75 ethyl oleate:Tween 80/Span 20

At the first stage a linear increase in the ultrasonic velocity is observed (Fig. 1(A)), with a breakpoint around 8 wt% of added water, after which the slope decreases. The ultrasonic attenuation at the first stage (Fig. 1(B)) decreases up to 7 wt% of added water, approximately.

Further addition of water results in a linear increase in the ultrasonic velocity up to 19 wt% where another breakpoint in the velocity line marks the transition between stages II and III. At the stage III the attenuation shows a sharp rise at water content between 20 and 25 wt%.

There is an increase in the ultrasonic velocity between 20 and 24 wt% of water, approximately (Fig. 1(B)). It remains then constant exhibiting some scattering of the data points, and begins to decrease until 45 wt% of added water. The ultrasonic attenuation does not change significantly within the resolution of the measurements at water content between 25 and 45 wt% and small scattering of the data points is observed. At 45 wt% of water the ultrasonic attenuation exhibits a drop and large scattering within the data points at higher concentrations of water, which provides evidence of a transition to stage IV. The evolution of the ultrasonic velocity profile with further addition of water shows little change from 45 wt% water in Fig. 1(B).

3.2. 50:50 ethyl oleate:Tween 80/Span 20 and 75:25 ethyl oleate:Tween 80/Span 20

The same transitions occur for 50:50 and 75:25 ethyl oleate:Tween 80/Span 20 (Figs. 2 and 3), with the exception of the transition from stage II to stage III for 75:25 ethyl oleate:Tween 80/Span 20. In this system, a direct transition from stage II to stage IV is observed with little evidence of significant presence of stage III. The transitions observed for 50:50 and 75:25 ethyl oleate:Tween 80/Span 20 occur at lower water concentration, compared with 25:75 ethyl oleate:Tween 80/Span 20.

3.3. Ultrasonic phase diagram

The concentrations of the components corresponding to transition between the stages are plotted on the pseudo-ternary phase diagrams in Fig. 4. The major phases, which can be found in ethyl oleate and Tween 80:Span 20 (3:2):water mixture at 25 °C at different water content (stages I–IV) are illustrated in Fig. 6. The triangles in Fig. 4 represent the transitions detected by the conductivity and viscosity measurements (Alany et al., 2001). Remarkably, the ultrasonic data show good agreement with the viscosity and conductivity measurements in same system and same temperature (Alany et al., 2001). The transition boundary between liquid crystalline phase and pseudo- bicontinuous determined by Alany et al. using phase-contrast microscopy and birefringence measurement coincides favourably with the transitions between stages III and IV on the 'ultrasonic phase diagram'. On other hand, the transition between microemulsion and liquid crystalline phase detected by cross-polarized microscopy occurs at slightly lower concentration of water than the transition between stages II and III on the ultrasonic phase diagram. This could be attributed to a difference in temperatures at which these transitions were measured, as the temperature was not controlled in the previous measurements with cross-polarized microscopy (Alany et al., 2001).

4. Discussion

4.1. Microscopic interpretation of ultrasonic profiles

4.1.1. Stage I

At this stage the ultrasonic velocity increases with concentration of water. Since change in compressibility is normally the main contribution to the change in the ultrasonic velocity (Eq. (3)), this indicates that the compressibility of the system decreases. The partial concentration increment of the ultrasonic velocity, a' (the slope of concentration dependence at stage I in Figs. 1–3(A)) is significantly higher (0.09–0.16) than the calculated value for thermal low frequency limit for nanoparticles containing bulk water in this concentration range (−0.08 to −0.04, Table 2). It is expected that at this stage the added water hydrates the hydrophilic groups of surfactant (Fig. 6). Therefore, the higher than expected for the bulk water value of partial concentration increment of the ultrasonic

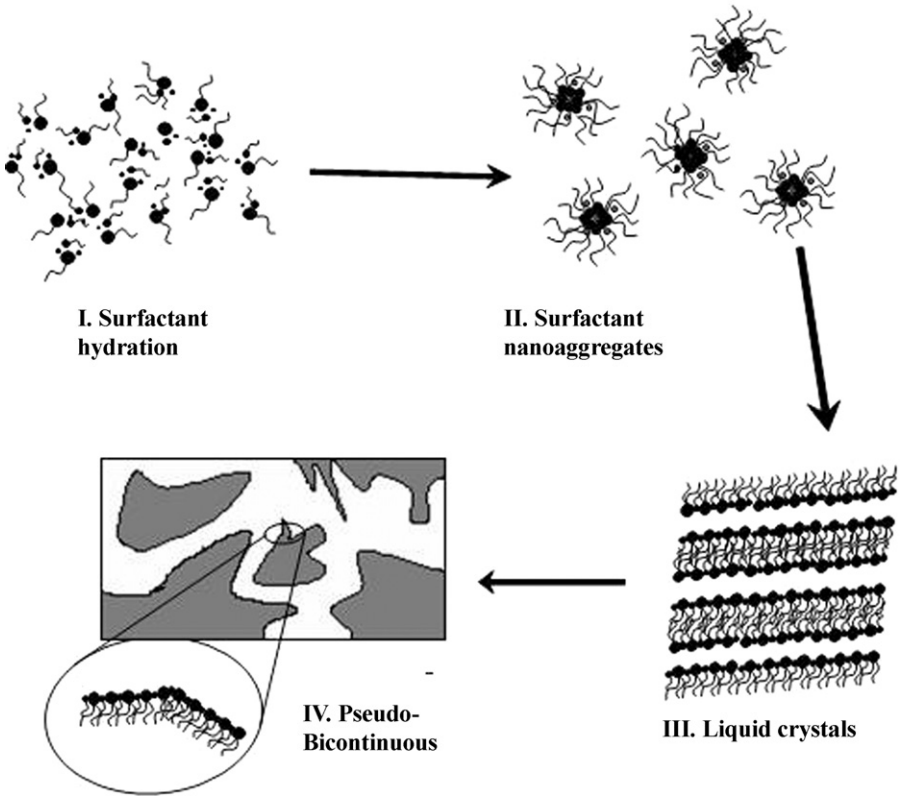

Fig. 6. Illustration of various phases presented in ethyl oleate and Tween 80:Span 20 (3:2):water mixture at 25 °C at different water content (stages I–IV).

velocity can be explained by lower compressibility of the hydration water (compared with the bulk water). This is in good agreement with the previous data on compressibility of water in the hydration state (Sarvazyan, 1991; Buckin, 1988; Buckin et al., 1989a,b). It also reflects the fact that compressibility of the bulk water is abnormally high because of a large structural contribution caused by structural changes associated with a change in pressure. This structural contribution to compressibility is attributed to a 'unique' structure of bulk water, where each molecule forms four hydrogen bonds with its neighbours (Nemethy and Scheraga, 1962). The hydration process partially 'destroys' this structure, thus decreasing the compressibility and increasing the velocity (Buckin, 1988). The partial concentration increment of the ultrasonic velocity of water increases with increase in concentration of surfactants. This is expected as the hydration should be more 'intense' in more concentrated systems.

There is a decrease in the ultrasonic attenuation at this stage, which is especially pronounced at high surfactant to oil ratio. This shall be expected due to the high level of attenuation in surfactant and oil mixture, which is 30 and more times higher than in pure water (Table 1). Therefore a simple replacement of the volume fraction of oil and surfactant mixture by water will reduce the attenuation level. However, the total decrease of attenuation cannot be explained by decrease in volume fraction of the surfactant and oil. This additional decrease could be attributed to a 'freezing' of the hydrophilic chains of the surfactant upon hydration, thus decreasing the high-frequency viscosity (shear and volume) and therefore the intrinsic attenuation of the liquid (Smyth et al., 1999, Litovitz and Davis, 1965; Stuehr and Yeager, 1965). Tween 80 contains 20 ethylene oxide groups as well as other polar groups (hydroxyl and ketone groups) which can form hydrogen bonds with water. We can suggest that binding of molecules of water with these groups, and possibly their bridging, results in freezing of some of their degrees of freedom. This may also contribute to the decrease in the compressibility of the system at this stage (large increase in the ultrasonic velocity).

4.1.2. Stage II

Beginning of the stage II is marked by both of breakpoint in the velocity line and sharp change in the ultrasonic attenuation profile, which are particularly clearly resolved at high-frequency (11 MHz) in 75:25 ethyl oleate:Tween 80/Span 20. The measured values of attenuation at this stage are higher than the additive sum of the intrinsic attenuation values in the dispersed and continuous phases estimated according to Eq. (1) and using data in Table 1 (shown as dotted baseline in Fig. 1 as an example). These differences in attenuation could be attributed to a formation of nanoaggregates that scatter the ultrasonic wave. For the estimation of the size of the particles from the ultrasonic attenuation, we assumed that (1) our dispersion consists of the continuous (oil/surfactant) medium and dispersed particles (water/surfactant); (2) all water in the system at this stage is incorporated into the dispersed particles; (3) the particles are spherical; and (4) the water in the particles has the same physical properties as the bulk (pure) water. Comparison of the experimental values with the dependence of attenuation on the particle size generated with PSize software module and data in Table 1 as described above (Fig. 6), allowed the estimation of the particle size. The size of water droplets in microemulsions (50:50 ethyl oleate:Tween 80/Span 20 and water, $w = 12\%$) and (25:75 ethyl oleate:Tween 80/Span 20 and water, $w = 14\%$) were 10–20 nm approximately (see Figs. 1 and 2). The obtained size of the dispersed particles shows frequency dependence, within the above limits. This can be attributed to two possible reasons: polydispersity of particles in our microemulsion as it was observed in other microemulsion systems (Moulik and Paul, 1998), and also the simplified model used in our ultrasonic particle sizing. For instance, the

assumption (4) is not strictly correct because at least some of the water in the system is bound to the hydrophilic atomic groups of surfactant heads which shall affect its physical properties as compared with the bulk water. The assumption (1) does not account for the existence of an intermediate layer of surfactant tails between both phases. Therefore the real particle size may deviate from the calculated one. Some uncertainty can also be attributed to a complexity in the definition of particle size in a system where the size of the intermediate layer is comparable with the whole particle size. Also, the assumption (2) does not account for some residual amount of water, which is not transferred from the continuous medium to microemulsion droplets when microemulsion is formed (according to our estimations in this case the size will be slightly higher, up to 25 nm). Our dynamic light scattering measurements in microemulsion at same water content at 50:50 oil/surfactant ratio provided the particle size around 15 nm, which is in the range estimated by HR-US ultrasonic method and close to the size of reverse micelles of Tween 80 in other microemulsion systems reported previously (Constantidines and Scalart, 1997; Shukla et al., 2004; Aizawa, 2009).

The measured partial concentration increment of the ultrasonic velocity, a', at this stage is about 60% lower compared with the stage I but it is higher than the partial concentration increment of the ultrasonic velocity expected for the bulk water. This can be explained by the fact that water at the stage II comprises at least two fractions: (A) hydration water accumulated at the stage I and (B) clusters of water which has properties and structure intermediate between the hydration water and the bulk water. This coincides well with the results obtained recently by Rane and Anderson (2008) who studied the state of dissolved water in triglycerides using theoretical simulations.

4.1.3. Stage III

There is sharp rise in the ultrasonic velocity and attenuation at the beginning of this stage. The increase in the attenuation followed by a plateau (Fig. 2B). The slope in the ultrasonic velocity curve at the beginning of this stage is extremely high compared with other stages and the value expected for the bulk water (Table 2). These changes indicate a transition of some amount of sample into a new state in a narrow concentration range. Alany et al. (2001) have found that surfactant forms liquid crystal structures (regular bilayers, Fig. 6) at this stage. Based on this we could suggest two possible explanations of the patterns of the ultrasonic velocity and attenuation.

Firstly, we could suggest that some of the geometric characteristics that the bilayer structures become to be comparable with the length of the ultrasonic wave (100–700 μm for our frequency range). This could produce a complex scattering pattern, which cannot be described by traditional ultrasonic scattering theory, valid for the long wavelength regime when the ultrasonic wavelength far exceeds the size of the particles (Povey, 1997). This effect can lead to complex profiles for velocity and attenuation. Secondly, we may suggest that the well ordered, continuous, rigid, liquid crystal bilayer structure provides an additional 'channel' for propagation of a secondary ultrasonic wave, directly through the structure. This could lead to existence of several ultrasonic waves and provide a basis for a complex behaviour of an 'effective' velocity and attenuation, which would depend on the measuring principles.

4.1.4. Stage IV

It is believed that a pseudo-bicontinuous structure exists, containing flexible and highly disorganised internal interfaces with no separation into continuous or dispersed phases at this stage (Fig. 6). This could explain the observed random scattering of the ultrasonic attenuation data. We should expect that the structure of this phase is very sensitive to stirring history and the scattering of the data points for ultrasonic attenuation at this stage can be explained by the shear effects which change the position of the random interfaces causing the scattering of the ultrasonic waves (Fig. 1(B)). We also can expect that the sizes of the structures in the system at this stage are comparable with the wavelength, which also should have an additional effect on ultrasonic attenuation and its sensitivity to the structural organisation.

4.2. State of water in the microemulsion. Comparison of ultrasonic data for water/ethyl oleate/Tween 80:Span 20 and IPM/Epikuron 200/n-propanol systems

Previously HR-US analysis of phase transitions in the similar type of non-ionic system (IPM/Epikuron 200/*n*-propanol/water) (Hickey et al., 2006), revealed three different states of water in microemulsion corresponding to hydration water (stage I), water in swollen reverse micelles (stage II) and bulk water in aqueous droplets surrounded by surfactant (stage III). This is in contrast to our present study of ethyl oleate/Tween 80:Span 20/water system, where only two stages in microemulsion (I and II) were detected, which followed by transition to the liquid crystalline state. Comparing the amount of water required to hydrate all the hydrophilic atomic groups of surfactant in both systems, we find that the end of the stage II approximately corresponds to minimum hydration of surfactant and co-surfactant in both system. In IPM:E200/*n*-propanol system the phosphatidylcholine head group is hydrated approximately by twelve water molecules (Small, 1967) with an additional two water molecules hydrating each hydroxyl group (–OH) in propanol molecule. This corresponds to the amount of water at the transition between stage II and stage III (Hickey et al., 2006). In ethyl oleate/water/Tween 80/Span 20 system the majority of hydration water is expected to be bound to ethylene oxide groups of Tween 80 ($-CH_2-O-CH_2-$) with minimum one water molecule per each of 20 groups in the surfactant (Shikata et al., 2006; Faraone et al., 1999) and the terminal hydroxyl groups (–OH) in Tween 80 and Span 20 (about two water molecules per each of 3 groups in the surfactants). Overall our estimations show that minimum 50 water molecules can be bound to one Tween 80 molecule/plus approximately 2.5 molecules to Span 20 (at Tween 80/Span 20 ratio of 3:2). This corresponds to 10, 16, and 23 wt% of water (approximately) in microemulsion with oil/surfactant ratios of 75:25, 50:50 and 25:75, respectively. These estimations are close or slightly exceed the amount of water in the system at the transition between the microemulsion (stage II) and the liquid crystalline phases (stage III). The instantaneous transition to liquid crystalline phase after the reaching of minimum hydration level of the surfactant indicates that the formation of bulk water in the droplets of ethyl oleate/Tween 80/Span 20 system is energetically unfavourable. In contrast to this in IPM:E200/*n*-propanol system the microemulsion state is followed by a coarse emulsion. The absence of liquid crystalline state probably provides favourable energetic for presence of bulk water in the microemulsion droplets at the stage III, when the hydration of surfactant and co-surfactant is complete. More detailed analysis of the hydration effects in the phase transitions in microemulsion will be subject of further publications.

5. Conclusion

Application of high-resolution ultrasonic spectroscopy has enabled the construction of a pseudo-ternary phase diagram of ethyl oleate/Tween 80 and Span 20/water system indicating phase transitions within microemulsion and other structures (liquid crystals, coarse emulsion and pseudo-bicontinuous phase). The transition zones determined by the ultrasonic meth-

ods agree well with those obtained previously using other techniques.

Changes in the ultrasonic parameters allowed evaluations on various structures present in the studied system and, in some cases, their qualitative characterisation. This included analysis of the state of water at various stages of microstructural reorganisation and particle size.

Overall, HR-US ultrasonic spectroscopy has proved to be a useful technique for characterisation of microemulsion systems. The ability to analyse these systems in titration mode is another advantages of this technique for characterisation of microemulsion systems.

Acknowledgments

We thank Ultrasonic Scientific Ltd. for providing instrumentation for this work and consultancy on the optimal measuring regimes, Dr. Jim Lyng, and Dr. Earl Waghorne for use of thermal analysis equipment. This work was supported by MASF315 grant from SFI Ireland and by a combined grant from Irish-American Partnership, Ultrasonic Scientific Ltd. and Aphton Biopharma.

References

Aboofazeli, R., Lawrence, M.J., 1993. Investigation into the formation and characterisation of phospholipid microemulsions. I. Pseudo-ternary phase diagrams of systems containing water–lecithin–alcohol–isopropyl myristate. Int. J. Pharm. 93, 161–175.

Aboofazeli, R., Barlow, D.J., Lawrence, M.J., 2000. Particle size analysis of concentrated phospholipid microemulsions. II. Photon correlation spectroscopy. AAPS Pharmsci. 2, 1–10 (article 19).

Aizawa, H., 2009. Morphology of polysorbate 80 (Tween 80) micelles in aqueous 1,4-dioxane solutions. J. Appl. Cryst. 42, 592–596.

Alany, R.G., Tucker, I.G., Davies, N.M., Rades, T., 2001. Characterising colloidal structures of pseudoternary phase diagrams formed by oil/water/amphiphile systems. Drug Dev. Ind. Pharm. 27, 31–38.

Allegra, J.R., Hawley, S.A., 1972. Attenuation of sound in suspensions and emulsions: theory and experiment. J. Acoust. Soc. Am. 51, 1545–1564.

Arleth, L., Pederson, J.S., 2001. Droplet polydispersity and shape fluctuations in AOT[bis(2-ethylhexyl)sulfosuccinate sodium salt] microemulsions studied by contrast variation small-angle neutron scattering. Phys. Rev. E 63, 061406–061423.

Austin, J.C., Holmes, A.K., Tebbutt, J.S., Challis, R.E., 1996. Ultrasonic wave propagation in colloid suspensions and emulsions: recent experimental results. Ultrasonics 34, 369–374.

Ballaro, S., Mallamace, F., Wanderlingh, F., 1980. Sound velocity and absorption in microemulsion. Phys. Lett. 77A, 198–202.

Benjamins, J., Thuresson, K., Nylander, T., 2005. Formation of a liquid crystalline phase from phosphatidylcholine at the oil–aqueous interface. Langmuir 21, 2804–2810.

Buckin, V., Kankia, B.I., Bulichov, N.V., Lebedev, A.V., Gukovsky, I.Ya., Chupnna, V.P., Sarvazyan, A.P., Williams, A.R., 1989a. Measurement of anomalously high hydration of (dA) • (dT), double helices in dilute solution. Nature 340, 321–322.

Buckin, V., Kankiya, B.I., Kazaryan, R.L., 1989b. Hydration of nucleosides in dilute aqueous solutions ultrasonic velocity and density measurements. Biophys. Chem. 34, 211–223.

Buckin, V., 1988. Hydration of nucleic bases in dilute aqueous solutions. Apparent molar, adiabatic and isothermal compressibilities, apparent molar volumes and their temperature slopes at 25 °C. Biophys. Chem. 29, 283–292.

Buckin, V., Kudryashov, E., 2002. Supersonic—high-resolution ultrasonic spectroscopy. Biochemistry 24, 25–27.

Buckin, V., O'Driscoll, B., 2002. Ultrasonic waves and material analysis: recent advances and future trends. Lab Plus Int. 16, 17–21.

Buckin, V., Kudryashov, E., O'Driscoll, B., 2002a. High-resolution ultrasonic spectroscopy for material analysis. Am. Lab. (Spectrosc. Persp. Suppl.) 28 (March), 30–31.

Buckin, V., O'Driscoll, B., Smyth, C., 2003. Ultrasonic spectroscopy for material analysis: recent advances. Spectrosc. Eur. 15, 20–25.

Buckin, V., Kudryashov, E., O'Driscoll, B., 2002b. An alternative spectroscopy technique for biopharmaceutical applications. Pharm. Technol. Eur. 14, 33–37.

Cheung, H.M., Qutubuddin, S., Edwards, R.V., Mann Jr., J.A., 1987. Light scattering study of oil-in-water microemulsions: corrections for interactions. Langmuir 3, 744–752.

Constantidines, P.P., Scalart, J.P., 1997. Formulation and physical characterization of water-in-oil microemulsions containing long-versus medium-chain glycerides. Int. J. Pharm. 158, 57–68.

Coupland, J.N., McClements, J.D., 2001. Droplet size determination in food emulsions: comparison of ultrasonic and light scattering methods. J. Food Eng. 50, 117–120.

Dukhin, A.S., Goetz, P.J., Wines, T.H., Somasundaran, P., 2000. Acoustic and electroacoustic spectroscopy. Colloid Surf. A: Physicochem. Eng. Aspects 173, 127–158.

Epstein, P.S., Carhart, R.J., 1953. The absorption of sound in suspensions and emulsions. I. Water fog in air. J. Acoust. Soc. Am. 25, 553–562.

Faraone, A., Magazu, S., Maisano, G., Migliardo, P., 1999. The puzzle of poly(ethylene oxide) aggregation in water: experimental findings. J. Chem. Phys. 110, 1801–1806.

Gao, Z., Choi, H., Shin, H., Park, K., Lim, S., Hwang, K., Kim, C., 1998. Physicochemical characterization and evaluation of a microemulsion system for oral delivery of cyclosporin A. Int. J. and evaluation of a microemulsion system for oral delivery of cyclosporin A. Int. J. Pharm. 161, 75–86.

Herrmann, N., Mc Clements, D.J., 1999. Ultrasonic propagation in highly concentrated oil-in-water emulsions. Langmuir 15, 7937–7939.

Hickey, S., Lawrence, M.J., Hagan, S.A., Buckin, V., 2006. Analysis of the phase diagram and microstructural transitions in phospholipid microemulsion systems using high-resolution ultrasonic spectroscopy. Langmuir 22, 5575–5583.

Hou, M.J., Kim, M., Shah, D.O., 1988. A light scattering study on the droplet size and interdroplet interaction in microemulsions of AOT–oil–water system. J. Colloid Interface Sci. 123, 398–412.

Hwang, S.R., Lim, S.J., Park, J.S., Kim, C.K., 2004. Phospholipid-based microemulsion formulation of all-trans-retinoic acid for parenteral administration. Int. J. Pharm. 276, 175–183.

Jian, X., Ganzuo, L., Zhiqiang, Z., Guowei, Z., Kejian, 2001. A study of the microstructure of CTAB/1-butanol/octane/water system by PGSE-NMR, conductivity and cryo-TEM. J. Colloid Surf. A: Physicochem. Aspects 191, 269–278.

Johannessen, E., Walderhaug, H., Balinov, B., 2004. Aqueous microemulsions of a fluorinated surfactant and oil studied by PFG-NMR: transformation from threadlike to spherical micelles. Langmuir 20, 336–341.

Kudryashov, E., Kapustina, T., Morrissey, S., Buckin, V., Dawson, K., 1998. The compressibility of alkyltrimethylammonium bromide micelles. J. Colloid Interface Sci. 203, 59–68.

Kudryashov, E., Smyth, C., Duffy, G., Buckin, V., 2000. Ultrasonic high-resolution longitudinal and shear wave measurements in food colloids: monitoring of gelation processes and detection of pathogens. Progr. Colloid Polym. Sci. 115, 287–294.

Lang, J., Djavanbakht, A., Zana, R., 1980. Ultrasonic absorption study of microemulsions in ternary and pseudoternarnary systems. J. Phys. Chem. 84, 1541–1547.

Lawrence, M.J., Rees, G.D., 2000. Microemulsion-based media as novel drug delivery systems. Adv. Drug Deliv. Rev. 45, 89–121.

Lehmann, L., Kudryashov, E., Buckin, V., 2004. Ultrasonic Monitoring of the gelitinisation of starch. Progr. Colloid Polym. Sci. 123, 136–140.

Letamendia, L., Pru-Lestret, E., Panizza, P., Rough, J., Scioritino, F., Tartaglia, P., Hashimoto, C., Ushiki, H., Risso, D., 2001. Relaxation phenomena in AOT–water–decane critical and dense microemulsions. Physica A 300, 53–81.

Litovitz, T.A., Davis, C.M., 1965. Structural and shear relaxation in liquids. In: Mason, W.P. (Ed.), Physical Acoustics. Part A. Properties of Gases, Liquids and Solutions, vol. II. Academic Press, pp. 281–349.

Lyng, J.G., Scully, M., McKenna, B.M., 2002. The influence of compositional changes in beef burgers on their temperatures and their thermal and dielectric properties. J. Muscle Foods 13, 123–142.

Mehta, S.K., Kawaljit, 1998. Isentropic compressibility and transport properties of CTAB–alkanol–hydrocarbon–water microemulsion systems. Colloids Surf. A 136, 35–41.

Moulik, S.P., Paul, B.K., 1998. Structure, dynamics and transport properties of microemulsions. Adv. Colloid Interface Sci. 78, 99–195.

Narang, A.S., Delmarre, D., Gao, D., 2007. Stable drug encapsulation in micelles and microemulsions. Int. J. Pharm. 345, 9–25.

Nemethy, G., Scheraga, H.A., 1962. Structure of water and hydrophobic bonding in proteins. I. A model for the thermodynamic properties of liquid water. J. Chem. Phys. 36, 3382–3400.

Patel, N., Schmid, U., Lawrence, M.J., 2006. Phospholipid-based microemulsions suitable for use in foods. J. Agric. Food Chem. 54, 7814–7824.

Povey, M.J., 1997. Ultrasonic Techniques for Fluid Characterisation. Academic Press, London.

Rane, S.S., Anderson, B.D., 2008. Molecular dynamics simulations of functional group effects on solvation thermodynamics of model solutes in decane and tricaprylin. Mol. Pharm. 5, 1023–1036.

Raman, I.A., Suhaimi, H., Tiddy, G.J.T., 2003. Liquid crystals and microemulsions formed by mixtures of a non-ionic surfactant with palm oil and its derivatives. Adv. Colloid Interface Sci. 106, 109–127.

Sarvazyan, A.P., 1991. Ultrasonic velocimetry of biological compounds. Annu. Rev. Biophys. Chem. 20, 321–341.

Shikata, T., Takahashi, R., Sakamoto, A., 2006. Hydration of poly(ethylene oxide)s in aqueous solution as studied by dielectric relaxation measurements. J. Phys. Chem. B 110, 8941–8945.

Shukla, A., Kiselev, M.A., Hoell, A., Neubert, R.H.H., 2004. Characterization of nanoparticles of lidocaine in w/o microemulsions using small-angle neutron scattering and dynamic light scattering. Ind. J. Phys. 63, 291–295.

Small, D.M., 1967. Phase equilibria and structure of dry and hydrated egg lecithin. J. Lipid Res. 8, 551–557.

Smyth, C., Dawson, K., Buckin, V., 1999. Ultrasonic analysis of heat-induced coagulation in calcium fortified milk. Progr. Colloid Polym. Sci. 112, 221–226.

Smyth, C., Kudryashov, E., O'Driscoll, B., Buckin, V., 2003. Sounding out pharmaceutical processes. JALA 8, 46–49.
Smyth, C., O'Driscoll, B., Lawrence, M.J., Hickey, S., O'Regan, T., Buckin, V., 2004. High-resolution ultrasonic spectroscopy: analysis of microemulsions. Pharm. Technol. Eur. 16, 31–34.
Stuehr, J., Yeager, E., 1965. In: Mason, W.P. (Ed.), Physical Acoustics, vol. 2A. Academic Press, San Diego, CA, pp. 351–358.
Urick, R.J., 1947. A sound velocity method for determining the compressibility of finely divided substances. J. Appl. Phys. 18, 983–987.
Warisnoicharoen, W., Lansley, A.B., Lawrence, M.J., 2000. Nonionic oil-in-water microemulsions: the effect of oil type on phase behaviour. Int. J. Pharm. 198, 7–27.
Waterman, P.C., Truell, R., 1961. Multiple scattering of waves. J. Math. Phys. 2, 512–537.
Wines, T.H., Dukhin, A., Somasundaran, P., 1999. Acoustic spectroscopy for characterizing heptane/H_2O/AOT reverse microemulsions. J. Colloid Interface Sci. 216, 303–308.